19

Finite Element Analysis of Desktop Machine Tools for Micromachining Applications

M. J. Jackson, L. J. Hyde, G. M. Robinson and W. Ahmed
Center for Advanced Manufacturing, College of Technology, Purdue University, West Lafayette, IN, USA

1. Introduction

The current interest in developing a manufacturing capability at the mixed scales is leading to a number of investigations concerned with the development of mesoscale machine tools (mMTs). The simulation of nanometric machining (Cook 1995, Inman 2001, Luo et al. 2003) and the effect of material microstructure (Komanduri et al. 2001 and Vogler et al. 2001) has led to the quest to construct machine tools capable of realizing 'bottom-up' fabrication processes in the general area of nanomanufacturing. The purpose of this paper is to investigate the use of a tetrahedral frame design to be used as a machine tool frame for meso, micro, and nanoscale machining applications. The problem with existing desk-top machine frames is the amount of vibration that is transmitted through the spindle, which affects the quality of surface finish and the dimensional accuracy imparted to the workpiece being machined. Owing to the way the spindle is mounted at the end of a cantilevered structure, low resonant frequencies can occur that are easily excited. In addition, the

Fig. 1. Tetrahedral machine tool frame.

amplitude of oscillation is more pronounced due to the geometry of the spindle mounting. An alternative approach is to design a vibration suppressing structure. When vibrations travel through a tetrahedral structure, they are canceled out or minimized due to the interference between the vibrating waves as they travel through the loops of the structure. The ability to minimize vibrations is needed because if the spindle oscillates during machining, an increase in the depth of cut will occur thus reducing the quality of surface finish, or dimensional accuracy of the machined part will be reduced significantly. Figure 1 shows the tetrahedral structure constructed for the purpose of this investigation. Modal analysis experiments were performed to investigate the structural response of the structure. Modal analysis experiments consisted of measuring the natural frequencies of the structure and deducing frequency response functions (F.R.F.) to determine the mode shapes of the structure. In addition, a finite element model (F.E.A.) model was constructed to compare to the experimental data, which also may be used for modeling any alterations to the design.

2. Analysis

The tetrahedral frame was initially analyzed from a numerical viewpoint using a closed-form solution and a numerical solution using finite element analysis.

2.1 Finite element model

Modal analysis of the tetrahedral structure using the finite element method was performed to obtain the natural frequencies and the mode shapes within the range of 0-8500 Hz, to compare to experimentally determined mode shapes. Modal analysis simulation was

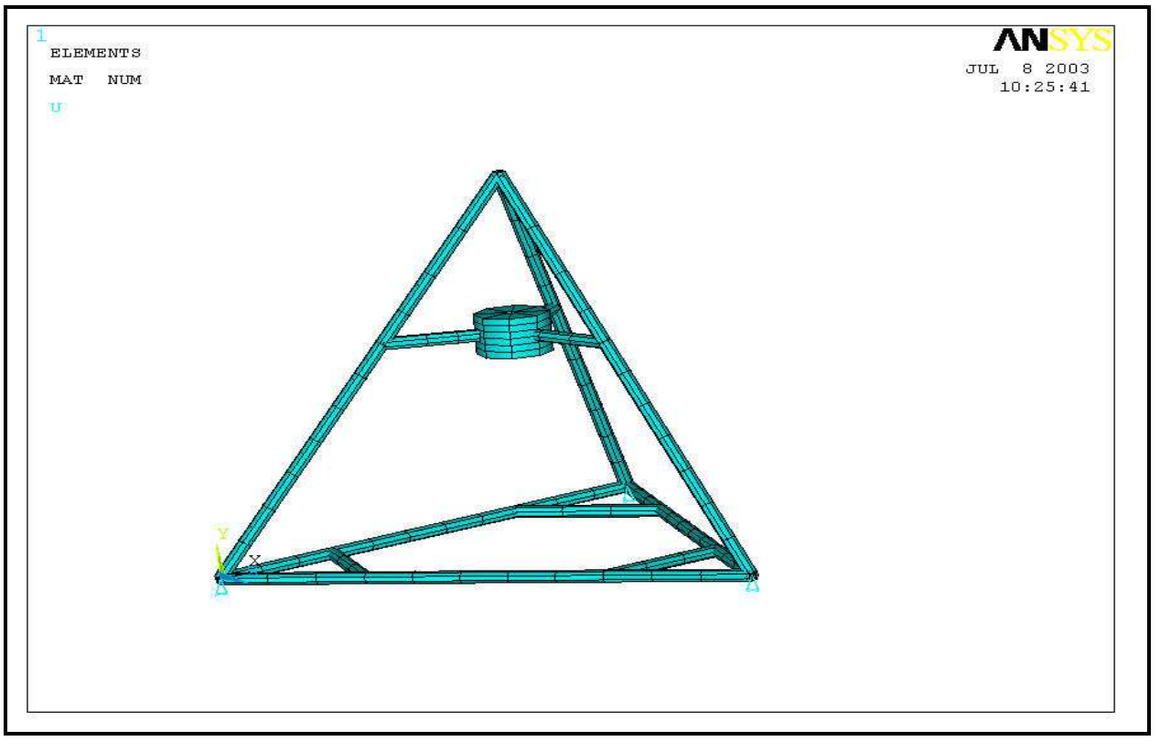

Fig. 2. Finite-element model of the machine tool frame.

performed using the finite element software package ANSYS 6.1. Model preparation was the first step in analyzing the modes of the tetrahedral structure (Stephenson 2002). This step involved creating a beam model of the structural members. The six bars that link the spheres and the reinforcement connections, which tie together the spindle sub-frame and the reinforcement bars were modeled using (ANSYS beam 188 elements), which have three translational degrees of freedom $U_x, U_y,$ and, U_z at each node and three rotational degrees of freedom θ_x, θ_y and θ_z. The three rotational degrees of freedom were needed to accurately simulate the boundary conditions at the vertices of the structure. The finite element model, shown in Figure 2 consists of 115 elements and 513 nodes. The material properties of cold rolled steel were used in the modal analysis.

Each of the beam elements used enabled a geometric cross-section to be assigned. Each of the structural beams was given a circular cross-section of 0.75" diameter. The spindle holder was modeled by using a 3.5" O.D. 0.70" I.D. beam. This allowed the spindle holder to rotate and bend in a smooth manner. To simulate the spheres located at each of the vertices of the structure, a mass element (ANSYS mass 21) was used. The actual spheres of the structure were weighed and mass moments of inertia were calculated for them, and then input into the mass element model. Beam elements were chosen over solid elements to reduce the computation time required to solve the problem.

2.2 Closed-form solution model

Sample calculations were performed to approximate the dynamic response of the tetrahedral structure. The purpose of these calculations is to obtain a continuous model of the structure instead of a finite element approximation.

The structure was modeled as four spheres at each of the vertices of the tetrahedron, with springs simulating the structural links between them. Equation 1 was the equation used to generate a mathematical model of the structure.

$$[M]*\ddot{X}+[K]*X=0 \tag{1}$$

Where, $[M]$ is the matrix of masses for each sphere, $\ddot{X}$ is the acceleration of each sphere, $[K]$ is the stiffness matrix for all of the structural links, and X is the displacement of each sphere. Equation 2 was used to model the stiffness (K) of each connecting rod only (axial displacements are considered in this formulation to decrease the complexity of the solution),

$$K=\frac{A*E}{L} \text{ where } \begin{matrix} A=cross-\text{sec}tionalarea \\ E=ModulusofElasticity \\ L=LengthofRods \end{matrix} \tag{2}$$

Since this structure was modeled as a 9 degree-of-freedom (d.o.f.) system, the methods listed by Inman (2001) were used. This method assumes that each of the d.o.f.'s can be modeled by the superposition of several single d.o.f. systems. The structure is a three-dimensional structure, where each equation had to be related to a global coordinate system similar to the methods used in finite element formulations. There were three degrees of freedom for the

top sphere and two degrees of freedom for the base spheres, which led to 9 possible natural frequencies. Damping was not considered in the mathematical modeling of this structure since it would create more difficulty in solving the equations.

2.2.1 Boundary conditions

The boundary conditions used for this structure had to allow the structure to translate along its base, but be constrained from movement in the vertical direction. To obtain these constraints, the top sphere was the only one that included a Z-axis component in the stiffness matrix, which allowed movement in the vertical direction. This allowed the vertical bars to move, which is required if the top sphere was allowed to oscillate. The base spheres did not include a vertical component since they were constrained from movement in the Z-direction. Since the displacement constraints existed only in the vertical direction, rigid body motion was to be expected, which led to three of the eigenvalues to be zero.

2.2.2 Free-body diagrams and derivation of equations of motion

Each of the spheres was modelled using a free-body diagram. The effect of gravity was neglected since it is taken into account by the equilibrium displacement of each of the structural links. The spring stiffness vectors corresponding to the direction illustrated the directions of displacement for the spheres. Damping was not considered in the mathematical modeling of this structure since it would create more difficulty in solving the equations and because it would not dramatically alter the natural frequencies of the structure. The equations of motion were derived from the free-body diagrams that were

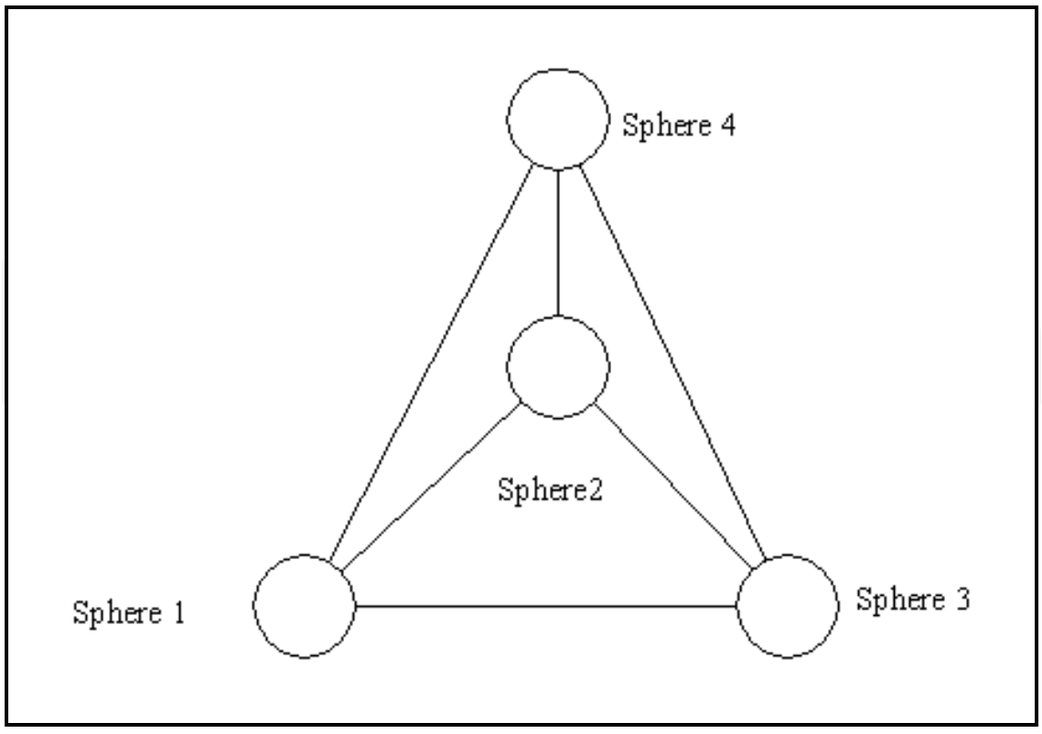

Fig. 3. Free-body diagram of the tetrahedral structure.

created for each of the spheres. There were two equations for each of the base spheres, and three equations for the top sphere. Since each of the links transmits oscillatory waves between the spheres, Newton's third law was used to simulate how each of the spheres responded to the force transmitted. Newton's third law of motion states that a body acted upon by a force will respond with an equal and opposite force to achieve equilibrium.

The first step to deriving a mathematical model was to relate the motion of each bar to a local X-Y-Z coordinate system. A brief example of how the equations for base sphere 1 were developed is shown. This example relates the motion for the links between sphere 1 and the spheres adjacent to it.

The free-body diagram shown in Figure 3 can be described using a set of local co-ordinate systems for each sphere connected to a global co-ordinate system connected by a series of rods. The system is shown in Figure 4.

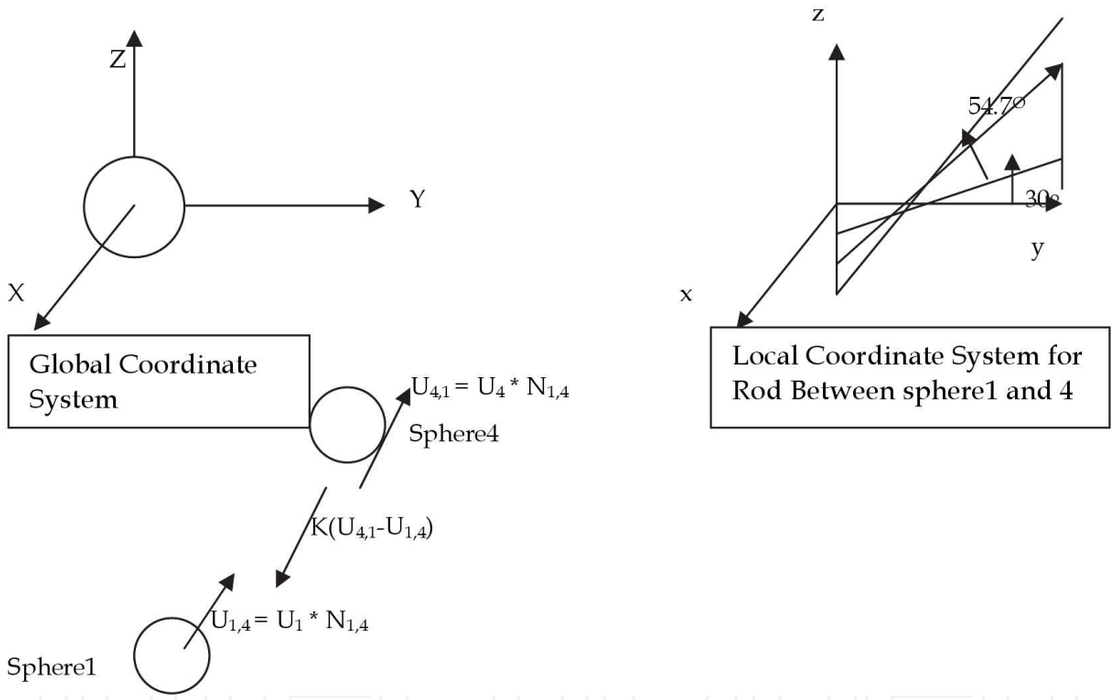

Fig. 4. Local and global co-ordinate system describing the relationship between spheres and connecting rods in the tetrahedral machine tool structure.

Figure 4 shows that,

$$N_{1,4} = e_{xy} \times \cos(54.7^o) - e_z \times \sin(54.7^o) \tag{3}$$

$$e_{xy} = e_y \times \cos(30^o) - e_x \times \sin(30^o) \tag{4}$$

Substituting for e_{xy} yields,

$$N_{4,1} = (e_y \times \cos(30^o) - e_x \times \sin(30^o)) \times \cos(54.7^o) - e_z \times \sin(54.7^o) \tag{5}$$

$$U_1 = (e_x x_1 + e_y y_1) \tag{6}$$

$$U_4 = (e_x x_4 + e_y y_4) \tag{7}$$

$$U_{1,4} = U_1 \bullet N_{1,4} \tag{8}$$

$$U_{4,1} = U_4 \bullet N_{1,4} \tag{9}$$

Equation 10 involves taking the dot product between the unit vector U_1 and $N_{1,4}$ to give,

$$U_{1,4} = (e_x \times x_1 + e_y \times y_1) \bullet ((e_y \times \cos(30^o) - e_x \times \sin(30^o)) \times \cos(54.7^o) + e_z \times \sin(54.7^o))$$

$$U_{1,4} = (-x_1 \times \sin(30^o) + y_1 \times \cos(30^o)) \times \cos(54.7^o) \tag{10}$$

Equation 11 involves taking the dot product between the unit vector U_4 and $N_{1,4}$ and reducing to give,

$$U_{4,1} = (e_x \times x_4 + e_y \times y_4 + e_z \times z_4) \bullet ((e_y \times \cos(30^o) - e_x \times \sin(30^o)) \times \cos(54.7^o) + e_z \times \sin(54.7^o))$$

That becomes,

$$U_{4,1} = (-x_4 \times \sin(30^o) + y_4 \times \cos(30^o)) \times \cos(54.7^o) + z_4 \times \sin(54.7^o) \tag{11}$$

Now writing the force balance,

$$F_{4,1} = K(U_{41} - U_{14}) \tag{12}$$

Thus Equation 12 becomes,

$$F_{4,1} = K[(-x_4 + x_1) \times \sin(30^o) \times \cos(54.7^o) + (y_4 - y_1) \times \cos(30^o) \times \cos(54.7^o) + z_4 \times \sin(54.7^o)] \tag{13}$$

The local equation of motion for the rod between sphere 1 and sphere 2 is shown in Figure 5. Figure 5 shows that,

$$N_{1,2} = -e_x \times \sin(60^o) + e_y \times \cos(60^o) \tag{16}$$

$$N_{2,1} = -e_x \times \sin(60^o) + e_y \times \cos(60^o) \tag{17}$$

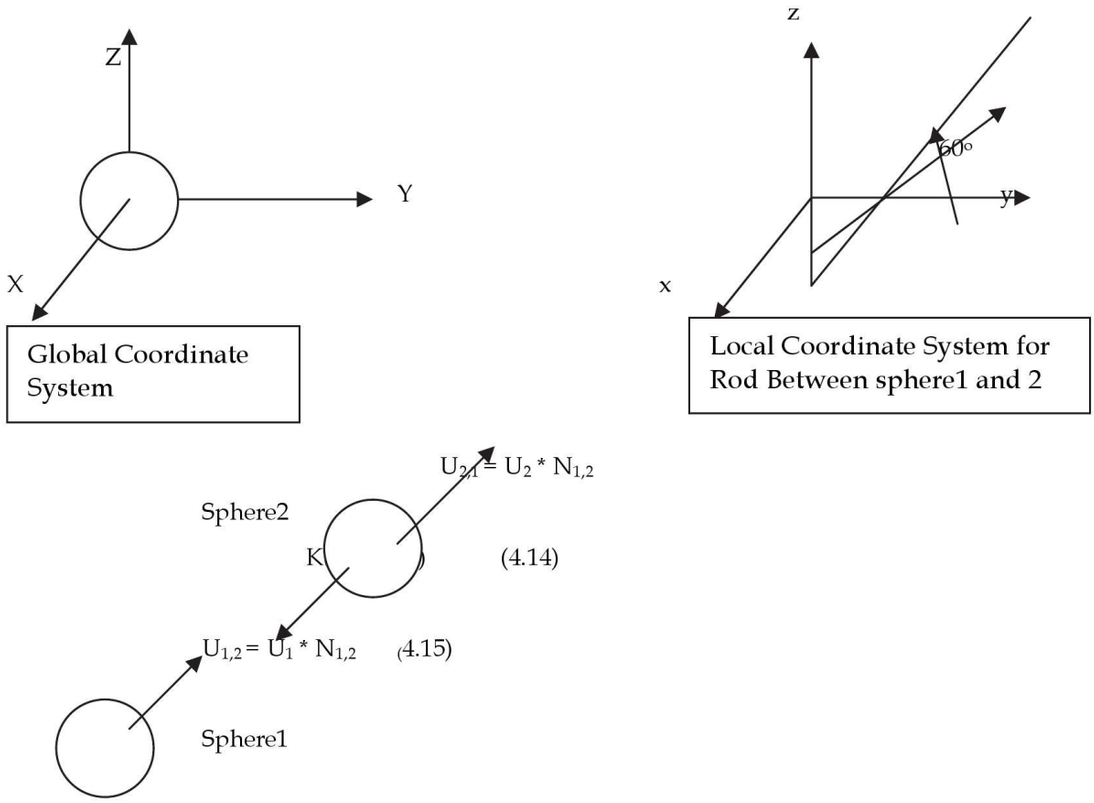

Fig. 5. Local and global co-ordinate system describing the relationship between spheres 1 and 2 and connecting rods in the tetrahedral machine tool structure.

$$U_1 = (e_x x_1 + e_y y_1) \tag{18}$$

$$U_2 = (e_x x_2 + e_y y_2) \tag{19}$$

$$U_{1,2} = U_1 \bullet N_{1,2} \tag{20}$$

$$U_{2,1} = U_2 \bullet N_{2,1} \tag{21}$$

$$U_{1,2} = (e_x \times x_1 + e_y \times y_1) \bullet (-e_x \times \sin(60^o) + e_y \times \cos(60^o)) \tag{22}$$

$$U_{2,1} = (e_x \times x_2 + e_y \times y_2) \bullet (-e_x \times \sin(60^o) + e_y \times \cos(60^o)) \tag{23}$$

Equation 23 reduces to,

$$U_{2,1} = (-x_2 \times \sin(60^o) + y_2 \times \cos(60^o)) \tag{24}$$

Now writing the force balance:

$$F_{2,1} = K(U_{2,1} - U_{1,2}) \tag{25}$$

Thus, Equation 25 becomes:

$$F_{2,1} = K[(-x_2 + x_1) \times \sin(60^o) + (y_2 - y_1) \times \cos(60^o)] \tag{26}$$

The local equation of motion for the rod between sphere 1 and sphere 3 is shown in Figure 6.

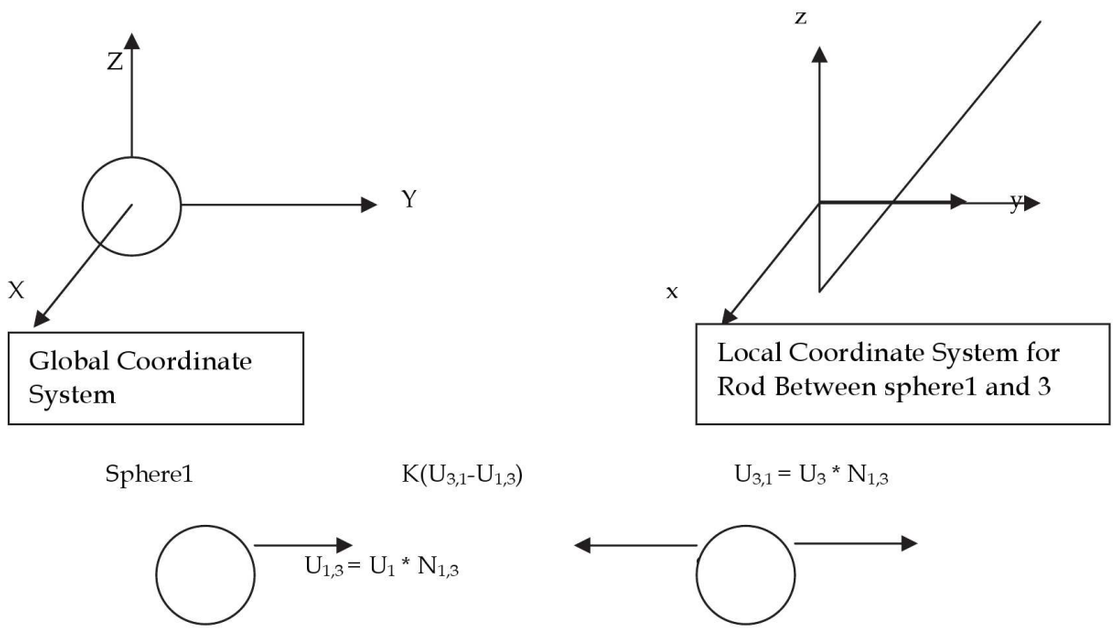

Fig. 6. Local and global co-ordinate system describing the relationship between spheres 1 and 3 and connecting rods in the tetrahedral machine tool structure.

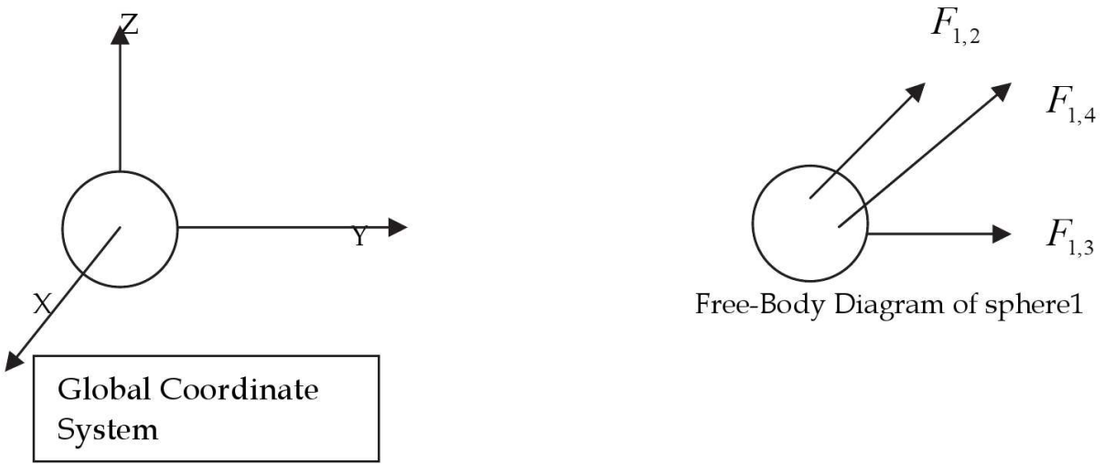

Fig. 7. Global co-ordinate system representing the tetrahedral machine tool structure in the form of a rod and sphere free-body diagram.

Now that the local equations of motion have been derived, the global system of equations must be defined. Summing forces in the X, and Y directions accomplish this task. The Z-

direction is not considered since the sphere is restricted from movement in this direction. Figure 7 shows the arrangement for the definition of the global co-ordinates of rods and spheres.

$$F_{3,1} = K(y_3 - y_1) \tag{27}$$

$$\sum F_{x1} = -F_{1,2} \times \cos(30^o) - F_{1,4} \times \cos(54.7^o) \times \sin(30^o) = M_1 \times \ddot{x}_1 \tag{28}$$

Substituting equations Equation 13, and Equation 26 yields,

$$\begin{aligned} &-K \times \cos(30^o) \times [(-x_2 + x_1) \times \sin(60^o) + (y_2 - y_1) \times \cos(60^o)] \\ &-K \times \cos(54.7^o) \times \sin(30^o) \times [(-x_4 + x_1) \times \sin(30^o) \times \cos(54.7^o) + \\ &(y_4 - y_1) \times \cos(30^o) \times \cos(54.7^o) + z_4 \times \sin(54.7^o)] = M_1 \times \ddot{x}_1 \end{aligned} \tag{29}$$

D'Alembert's Principle is used so that the equation will be in the correct form for substituting into the stiffness matrix, K, and into the mass matrix, M, thus,

$$\begin{aligned} &K \times \cos(30^o) \times [(-x_2 + x_1) \times \sin(60^o) + (y_2 - y_1) \times \cos(60^o)] \\ &K \times \cos(54.7^o) \times \sin(30^o) \times [(-x_4 + x_1) \times \sin(30^o) \times \cos(54.7^o) + \\ &(y_4 - y_1) \times \cos(30^o) \times \cos(54.7^o) + z_4 \times \sin(54.7^o)] + M_1 \times \ddot{x}_1 = 0 \end{aligned} \tag{30}$$

Summing forces in the Y-direction gives,

$$\sum F_{y1} = F_{1,2} \times \cos(60^o) + F_{1,3} + F_{1,4} \times \cos(54.7^o) \times \cos(30^o) = M_1 \times \ddot{y}_1 \tag{31}$$

Substituting equations Equation 13, and Equations 26 and 27 yields,

$$\begin{aligned} &K \times \cos(60^o) \times [(-x_2 + x_1) \times \sin(60^o) + (y_2 - y_1) \times \cos(60^o)] \\ &+K \times [(y_3 - y_1)] \\ &+K \times \cos(54.7^o) \times \cos(30^o) \times [(-x_4 + x_1) \times \sin(30^o) \times \cos(54.7^o) + \\ &(y_4 - y_1) \times \cos(30^o) \times \cos(54.7^o) + z_4 \times \sin(54.7^o)] = M_1 \times \ddot{y}_1 \end{aligned} \tag{32}$$

Again, D'Alembert's Principle is used so that the equation will be in the correct form for substituting into the stiffness matrix, K, and the mass matrix, M,

$$\begin{aligned} &-K \times \cos(60^o) \times [(-x_2 + x_1) \times \sin(60^o) + (y_2 - y_1) \times \cos(60^o)] \\ &-K \times [(y_3 - y_1)] \\ &-K \times \cos(54.7^o) \times \cos(30^o) \times [(-x_4 + x_1) \times \sin(30^o) \times \cos(54.7^o) + \\ &(y_4 - y_1) \times \cos(30^o) \times \cos(54.7^o) + z_4 \times \sin(54.7^o)] + M_1 \times \ddot{y}_1 = 0 \end{aligned} \tag{33}$$

Equations 30 and 33 may be substituted into the stiffness matrix K and the mass matrix M.

2.2.3 Solution of matrices

After the equations for the 9 degrees-of-freedom were written, they were solved to find the natural frequencies of vibration. Two matrices were built, one for the mass matrix [M], and a stiffness matrix [K]. Once the matrices were built the eigen function was used to solve the eigenvalues and eigenvectors. Once the eigenvalues were solved, the square root was taken followed by dividing by 2π, which yielded the natural frequencies of the system in units of Hertz. There were three zero eigenvalues, which was expected since rigid-body motion in the X and Y directions and rotation in the XY plane was allowed. There were also two repeated eigenvalues that occurred due to symmetry of the structure. This was considered to be trivial since the eigenvectors would not be used for generating mode shapes. A list of the natural frequencies found from the mathematical model is shown in Table 1.

Mode set	Frequency (Hertz)
0	0
1	0
2	0
3	0
4	19.6
5	19.6
6	33.0
7	34.6
8	34.6
9	50.2

Table 1. Natural frequencies generated for the tetrahedral machine tool structure based on the results using the closed-form model.

2.3 Model verification

A comparison of the closed-form solution and the simplified finite-element model of the structure was performed. This was conducted to determine whether the finite element software, ANSYS, would yield accurate results that would be comparable to the mathematical model. The bar model from ANSYS consists of 6 bar elements and 4 mass elements, which are located at the vertices of the structure. The bar element was a beam 3 element, which only allows movement along its axis, thus tension or compression. This was used since the mathematical model was formulated in this manner. The structure was constrained from movement in the U_y direction and rotations about the Z-axis, and the X axis. The model and the constraints are shown in Figure 8.

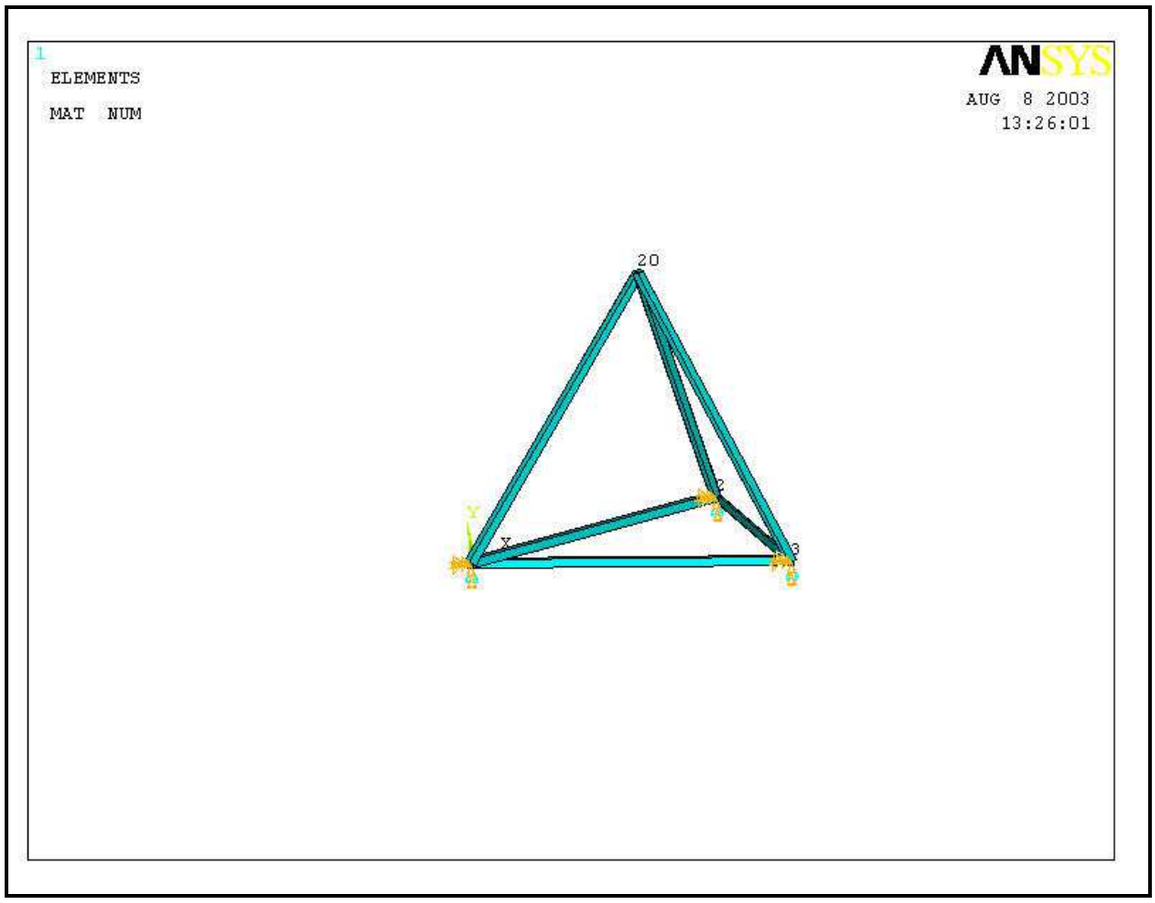

Fig. 8. A simple bar model to compare to the closed-form solution.

Finite element bar model (ANSYS)		Closed-form solution model		% Difference
Mode set	Frequency	Mode set	Frequency	
	(Hz)		(Hz)	
1	0	1	0	0%
2	0	2	0	0%
3	0	3	0	0%
4	23.5	4	19.6	-20%
	Not available	5	19.6	0%
	Not available	6	33.0	0%
5	37.1	7	34.6	-7%
	Not available	8	34.6	0%
6	51.4	9	50.2	-2%

Table 2. Comparison of finite element bar model to the closed-form solution.

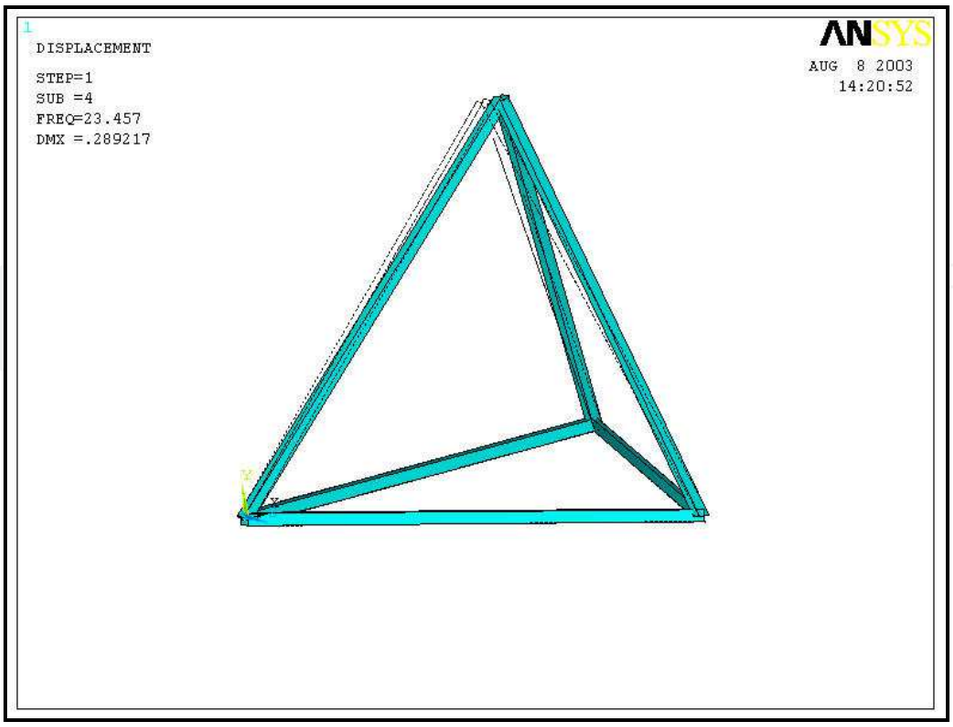

Fig. 9. Finite-element bar model showing displacement of the structure at a frequency of 23.5 Hz.

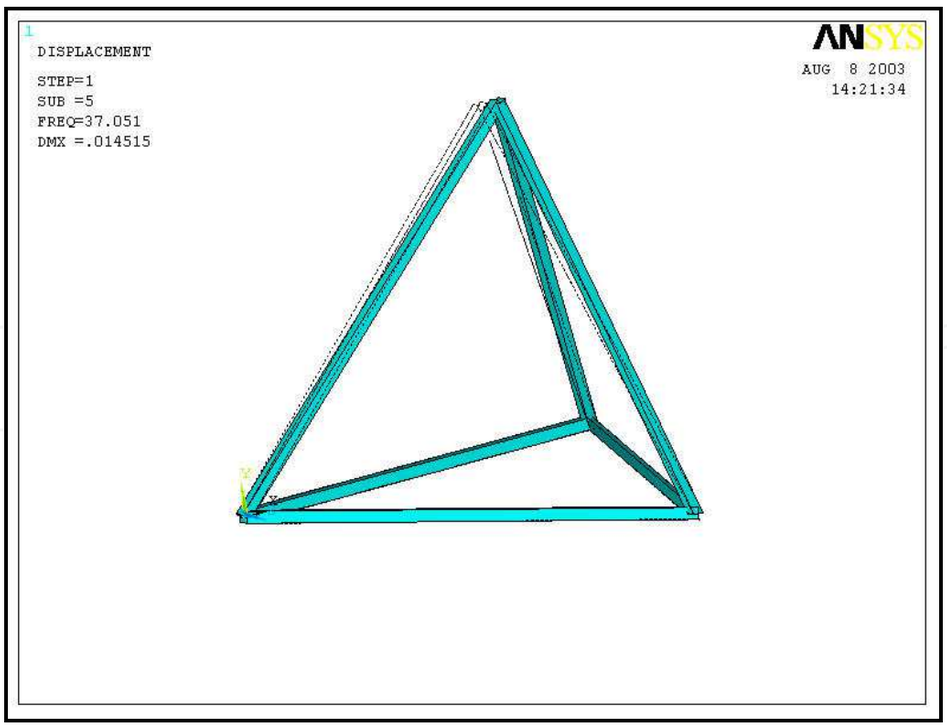

Fig. 10. Finite element bar model showing displacement of the structure at a frequency of 37 Hz.

Table 2 lists the frequencies found from the finite element model and compares them to the closed-form solution. Both models show three rigid body modes and have three frequencies that are similar. Only six frequencies were found from ANSYS since it only had six degrees of freedom, one for each of the bar elements. In addition, it can be seen as the frequencies increase the percentage difference decreases. The finite element beam model built to compare with the measured model was not used to compare with the closed-form solution because it did not include any bending modes, therefore the two do not correlate. However the closed-form solution is useful, since it proved that ANSYS compares accurately using a simplified bar model, and should compare well to the measured model.

Since the finite element model compares reasonably well with the closed-form solution, the mode shapes that were generated from ANSYS are shown in Figures 9-11.

It can be shown from Figure 9 and Figure 10 that the top vertex oscillates along one of the rods. One of the upper rods shortens, whereas the opposing rods rotate about the base vertices.

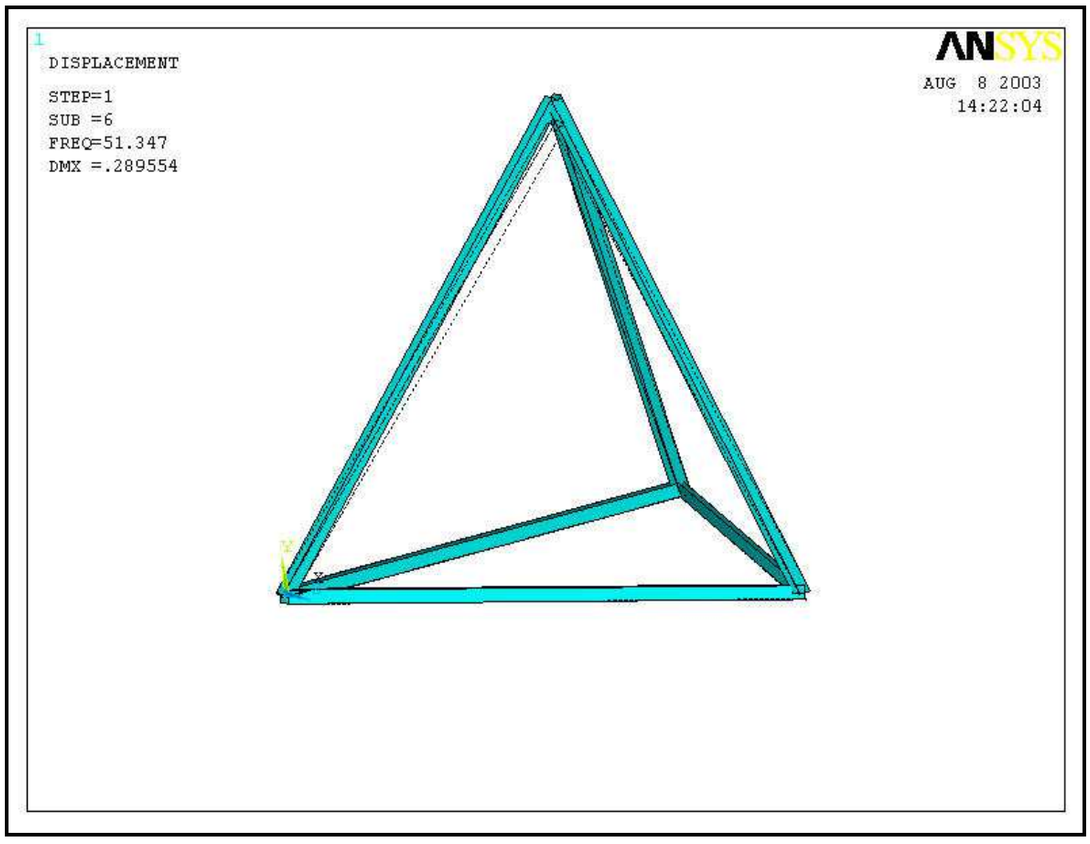

Fig. 11. Finite element bar model showing displacement of the structure at a frequency of 51.3 Hz.

Figure 11. Illustrates how the structure oscillates at 51.3 Hz. It can be seen that each of the upper rods elongates thus causing the top vertex to increase its height.

3. Experimental

The impact hammer test has become a widely used device for determining mode shapes. The peak impact force is nearly proportional to the mass of the head of the hammer and its impact velocity. The load cell in the head of the hammer provides a measure of the impact force. This data is used to compute the frequency response function (F.R.F.). The use of an impact hammer avoids the mass-loading problem and is much faster to use than a shaker. An impact hammer consists of a hammer with a force transducer built into the head of the hammer. The hammer is used to impart an impact to the structure and excite a broad range of frequencies. The impact event is supposed to approximate a Dirac-delta function [2].

3.1 Experimental method

The tetrahedral structure [6] was placed on a granite table in order to gain accelerometer measurements, thus the structure was allowed to freely move longitudinally and transversely across the table. The roving accelerometer approach was used for all of the measurements. The center of the spindle frame was used as the excitation point for the structure. The accelerometer was placed at various points of interest about the structure.

3.2 Experimental procedure

The data acquisition system was set up to take data at a sampling frequency, F_s, of 17000 Hz for 8192 points with a delay of 100 points. The voltage range on both channels was set to +\- 5 volts. Data was acquired in the time domain by averaging 8 ensembles and storing the data in binary format for use by Matlab software. This data was used to find the natural frequencies of the structure and their corresponding mode shapes. While applying the roving accelerometer technique, the structure was excited in the center of the spindle sub-frame and data was acquired at points 1-28. Before the time domain data was stored, it was filtered to remove any aliasing that might have occurred from under-sampling. This was accomplished by installing an analog filter between the power supply and the P.C. The frequency was set at 8500 Hz, which corresponds to the Nyquist frequency of the measured data. After the data was recorded, it was translated into a binary file to be fed into Matlab software. The method used on the F.R.F. data of a multi-degree-of-freedom structure is the single-degree-of-freedom-curve-fit (S.D.O.F.). In this method the frequency response function for the compliance is sectioned off into frequency ranges bracketing each successive peak. Each peak is analyzed by assuming that it is the F.R.F. of a single-degree-of-freedom system. This assumes that in the vicinity of resonance the F.R.F. is dominated by that single mode. Once the frequency response function (F.R.F.) is completed for the chosen data points of a structure, it is then appropriate to compute the natural frequencies, damping ratios and modal amplitudes with each resonant peak. An example of one of the F.R.F.'s is shown in Figure 13. The damping ratio associated with each peak is assumed to be the modal damping ratio Zeta, ξ. The modal damping ratio Zeta is related to the frequencies corresponding to Equation 34.

$$\left|H(\omega_a)\right| = \left|H(\omega_b)\right| = \frac{\left|H(\omega_d)\right|}{\sqrt{2}} \tag{34}$$

And $\omega_b - \omega_a = 2\zeta\omega_d$, so that

$$\zeta = \frac{\omega_b - \omega_a}{2\omega_d} \tag{35}$$

ω_d is the damped natural frequency at resonance such that ω_a and ω_b satisfy Equation 3. The condition of Equation 34 is termed the 3 dB down point. Both the natural frequency and the damping ratio Zeta may be found using this method. Once the values of ω_a and ω_b are determined, then ζ is found for the structure at the prescribed frequency (Equation 35). This method was used in the software to experimentally determine the damping and mode shapes. Figure 13 gives an example of F.R.F. data set that was found from the tetrahedral structure.

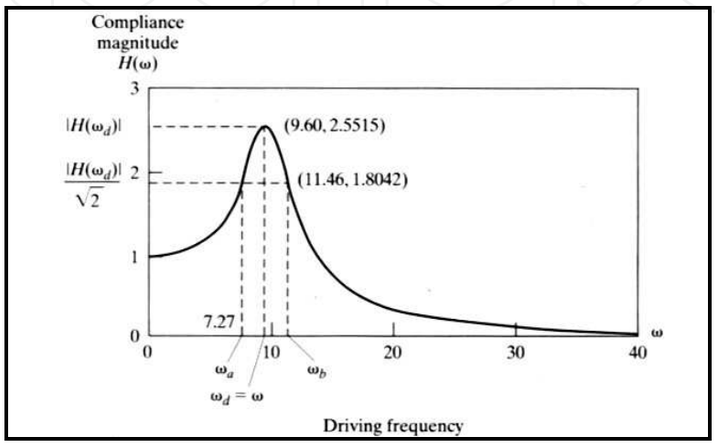

Fig. 12. Magnitude of the frequency response function, illustrating the calculation of the modal damping ratio by using the quadrature peak-picking method for lightly damped systems.

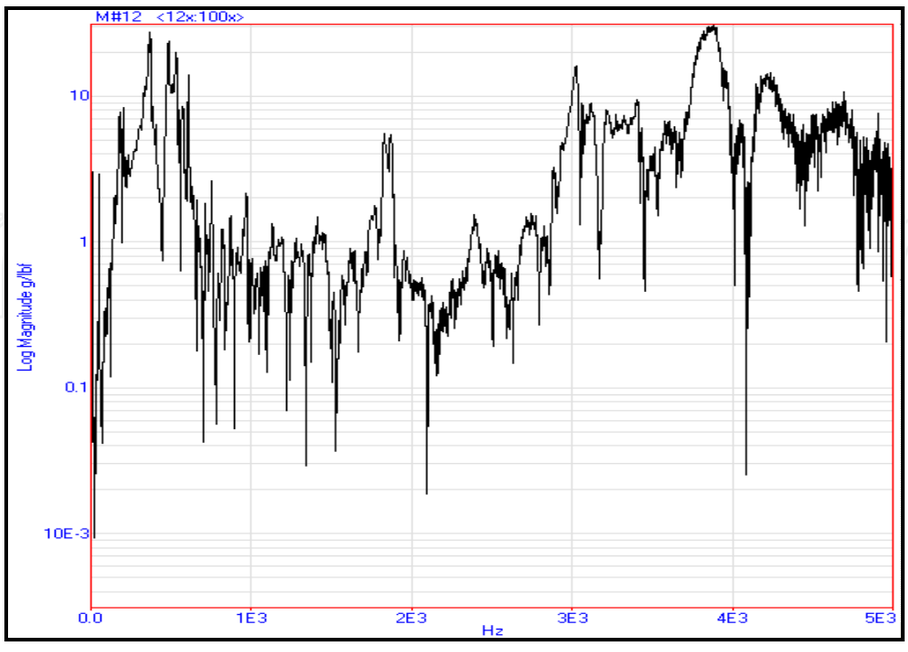

Fig. 13. Example of F.R.F. data set cut off at 5000 Hz.

3.3 Experimental analysis

Using the measured data obtained from Me-Scope software, a model was constructed and the data was used to find structural damping and mode shapes. At first it was thought that the data was too low since the operating frequencies of the spindle are above 4500 Hz. However the operating frequencies of the spindle could excite lower frequencies while machining. Therefore, this data is useful if the structure is excited at these frequencies by some other means, such as localized impacts the structure might experience during a machining operation. This is shown in the following series of illustrations at the chosen frequencies (Figures 15 –20). The measured data for each node was adjusted such that the axis of orientation corresponded with the orientation of the accelerometer.

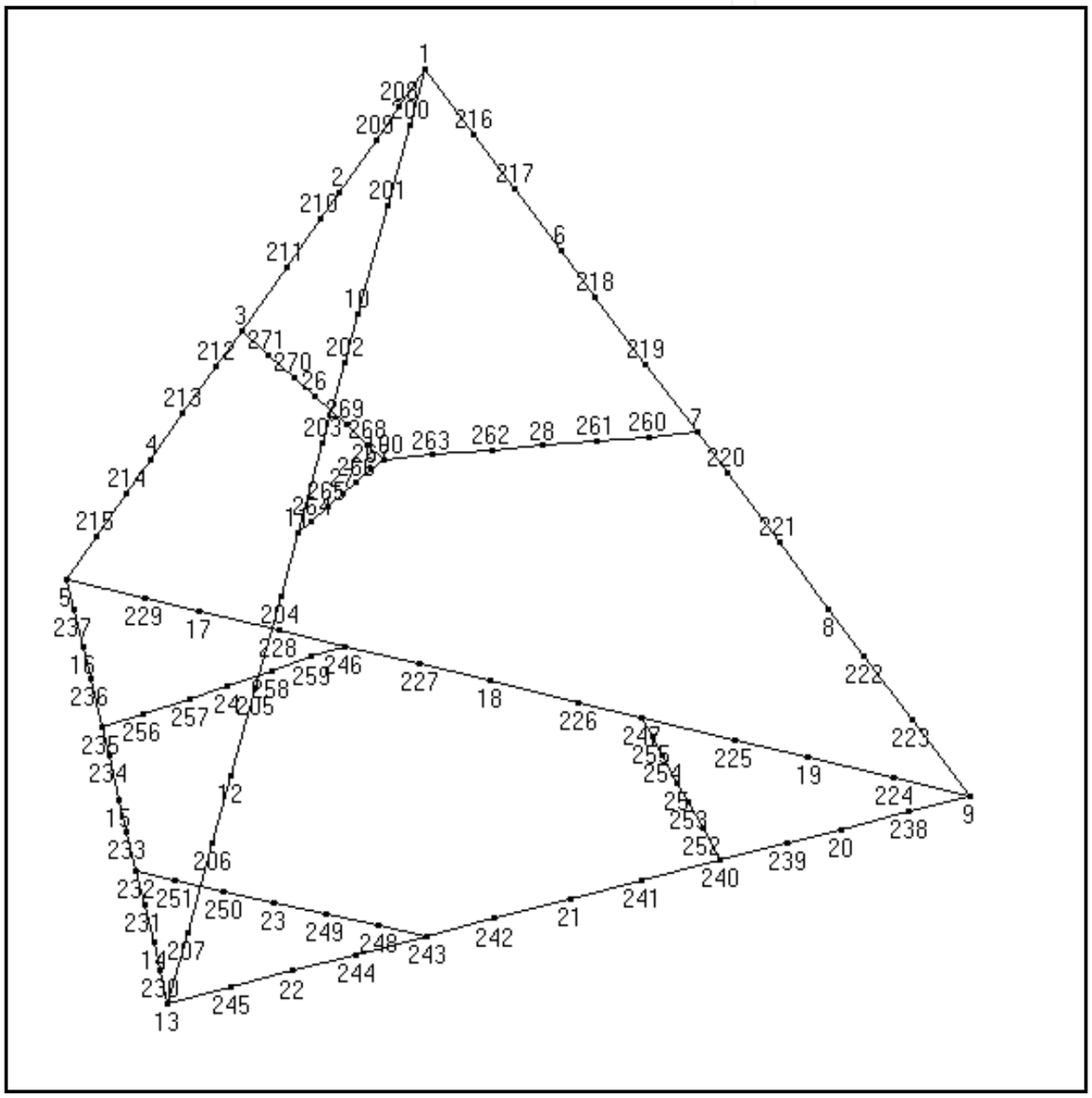

Fig. 14. Schematic diagram of the tetrahedral machine tool structure showing experimental points-of-measurement for determining mode shapes.

Figure 14 illustrates where mode shape measurements were taken during the experimental phase of this study (numbers 1-28 represent actual data points, whereas the other numbers were used for interpolation between measurement points.

4. Results and discussion

The measured data compared accurately with the finite element results. It was found that the position of the centre of the spindle proved to be a point inside the structure that experienced minimal oscillations. It appeared that the structure was kinematically balanced such that different parts of the structure had oscillations that were out of phase with other parts. The tetrahedral structure was analyzed in its working orientation. The results are tabulated in Table 1.

Measured data	Finite element results	
(Me-Scope software)	(ANSYS software)	% Difference
125	125	0%
203	200	1%
401	407	-1%
534	535	0%
601	600	0%
1070	1085	-1%
1820	1794	1%

Table 3. Comparison between measured and finite element calculations.

Not all of the results are listed, only those of interest. The first column is the measured natural frequency, followed by the finite element generated natural frequency in the second column. The observed modes of interest are shown in Figures 15-17. The following figures illustrate how the tetrahedral structure oscillates at various frequencies. The measured data mode shape is given first, followed by a corresponding finite element generated mode shape. As the frequency is increased, the results from the finite element model seem to diverge from the measured mode shapes. It is thought that as oscillation modes increase they tend to depart from Bernoulli beam theory upon which the finite element generated results depend. For most of the natural frequencies, the amount of oscillation of the spindle is small, or approximately zero, which is preferred since the amount of spindle oscillation from equilibrium is translated directly to the machined workpiece. The results from ANSYS above 1794 Hz did not coincide with what was measured, therefore no comparison was made. However, measured frequencies above 1820 Hz are shown because they are useful for future design revisions to the structure. Axial responses, as well as transverse responses, from the measured data were used to compare to the finite element results. Torsional data was ignored since it was not recorded using the accelerometer and the Me-Scope measurement software. It can be seen from the percent difference that the results from ANSYS have a natural frequency that resembles the measured results. However, they do not converge exactly instead the results oscillate about the measured data.

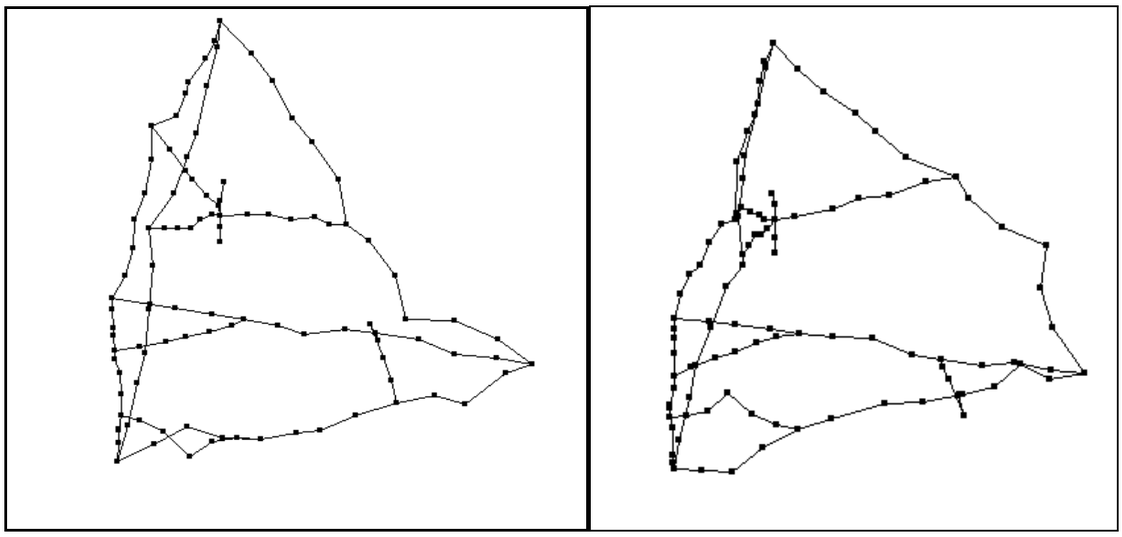

Fig. 15a. Me-Scope measured mode shape data (i.e., displacement) at a frequency of 125 Hz.

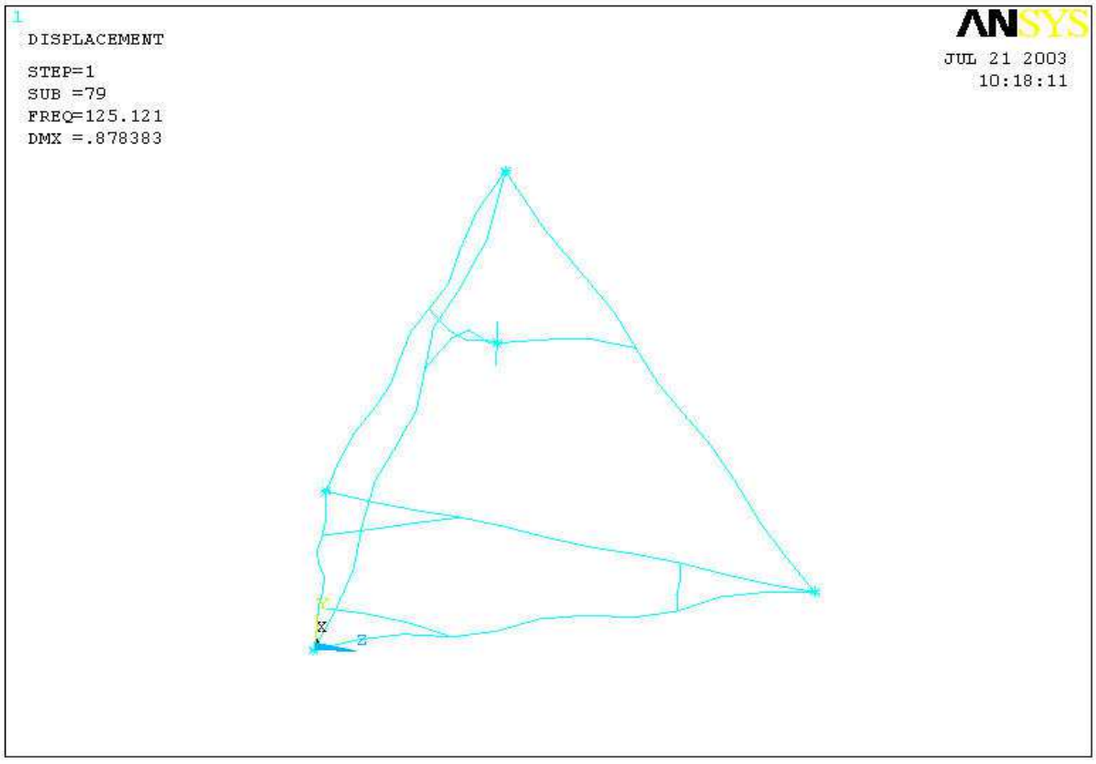

Fig. 15b. Finite element generated model of mode shape data (displacement) at a frequency of 125 Hz.

The measured mode shape data using ME-Scope software at a frequency of 125 Hz shows an axial deflection for the spindle frame. However, the spindle itself remains stationary. The ANSYS model shows bending in the spindle sub-frame. Both finite element models show axial bending modes in the structural bars.

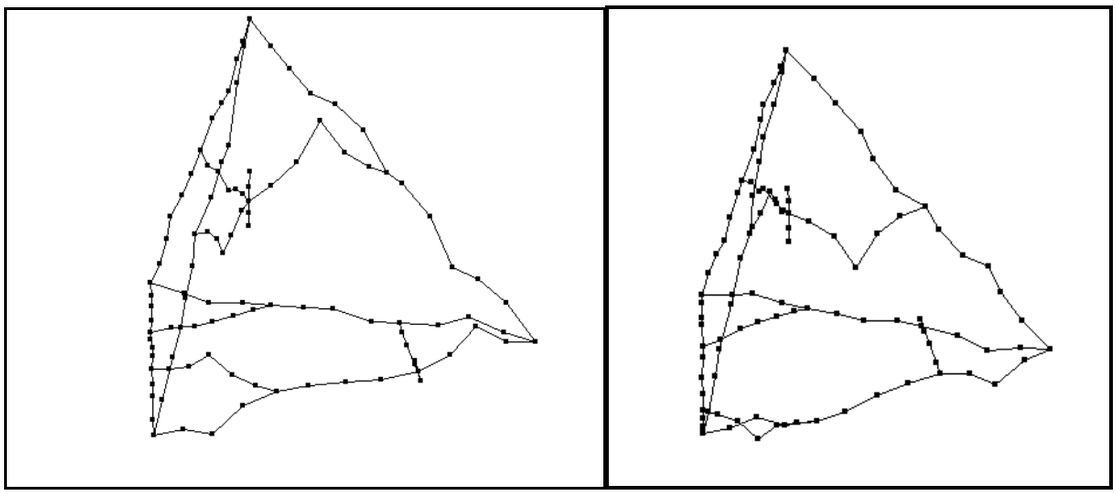

Fig. 16a. Me-Scope measured mode shape data (displacement) at a frequency of 232 Hz.

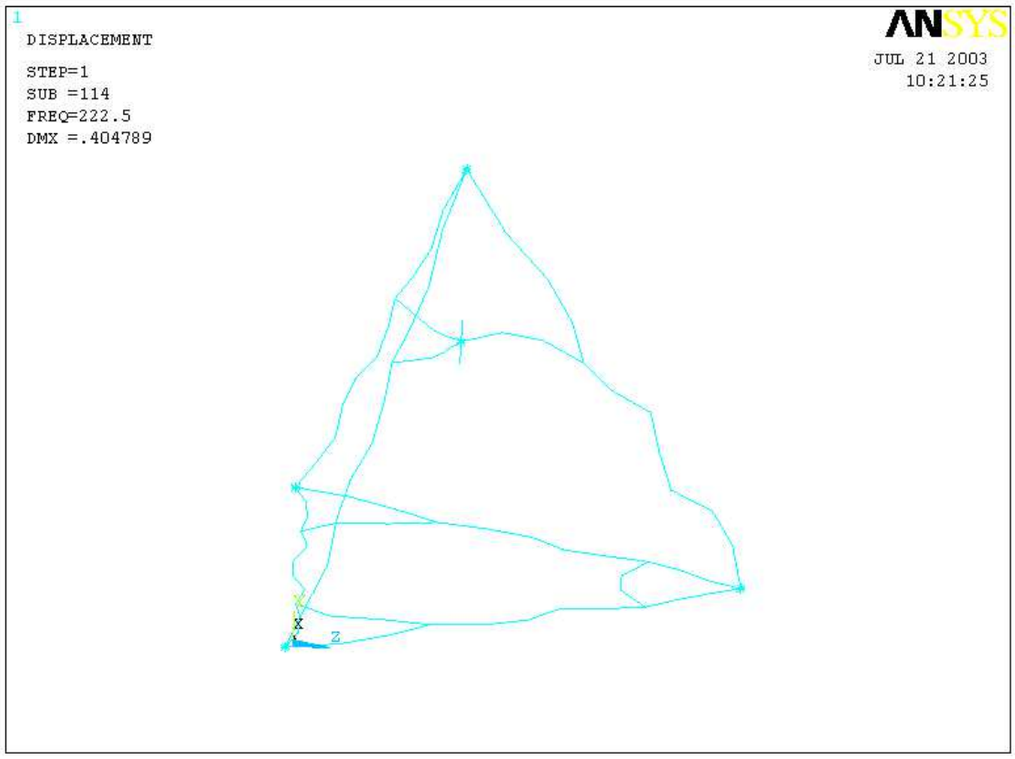

Fig. 16b. Finite element generated model of mode shape data (displacement) at a frequency of 222 Hz.

The measured mode shape at 232 Hz illustrates how the structure cancels out oscillations that are transmitted through the spindle. It is apparent from the measured mode shape as well as the finite element model, how various structural members are out of phase, which prevents any displacement of the spindle from its equilibrium position thus achieving a preferred effect for machining.

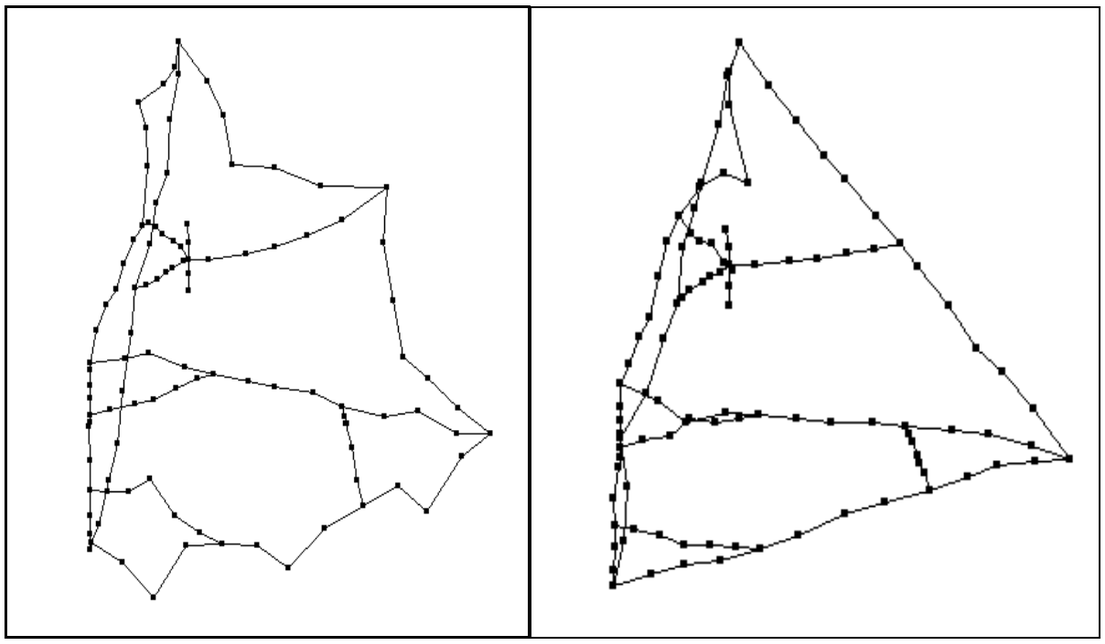

Fig. 17a. Me-Scope measured mode shape data (displacement) at a frequency of 1820 Hz.

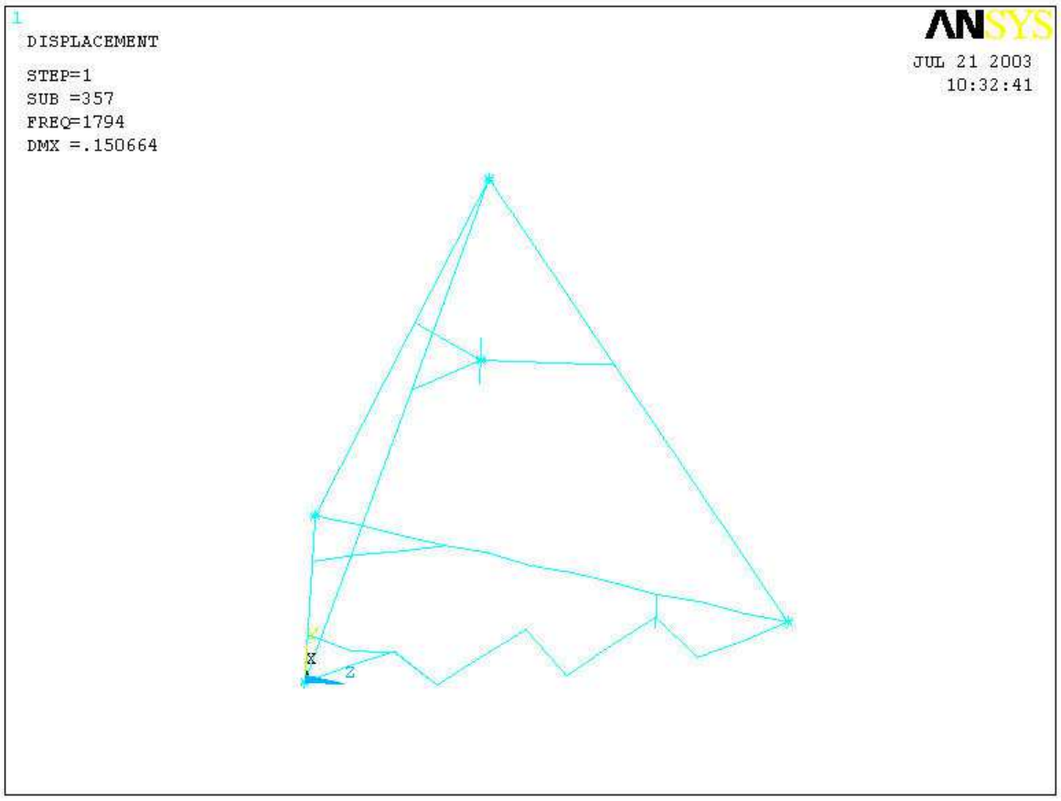

Fig. 17b. Finite element generated model of mode shape data (displacement) at a frequency of 1794 Hz.

The measured data vaguely coincides with the finite element model once the frequencies reach approximately 1800 Hz, as illustrated from the images from Me-Scope at 1820 Hz and the finite element results at 1794 Hz. For this reason the finite element results have been omitted above 1820 Hz. This may be due to inadequate modeling of the structural connections, but most likely due to Bernoulli beam theory not being applicable at these frequencies. The only characteristic that is common to both of the models is the restricted oscillation of the spindle. It can readily be seen from the following Figures 18 – 20 that there is virtually zero oscillation in the spindle at most of the measured frequencies, this is accompanied by the finite element model as well. The reason for omitting results above 4460 Hz is because the F.R.F. from the measured data was not clean, thereby resembling noise, which is not useful for an adequate conclusion to be made. This is because the impact hammer method of exciting a structure is limited to approximately 4000 Hz.

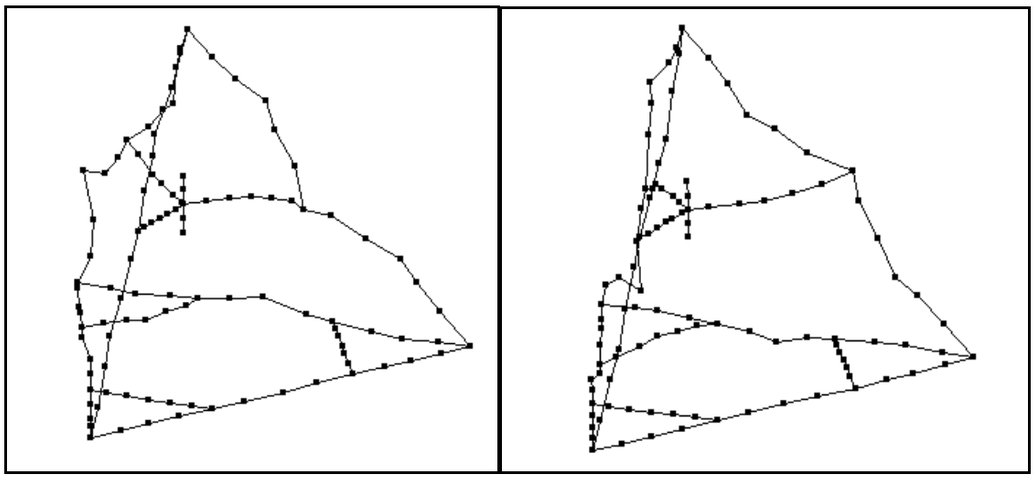

Fig. 18. Me-Scope measured mode shape data (displacement) at a frequency of 2890 Hz.

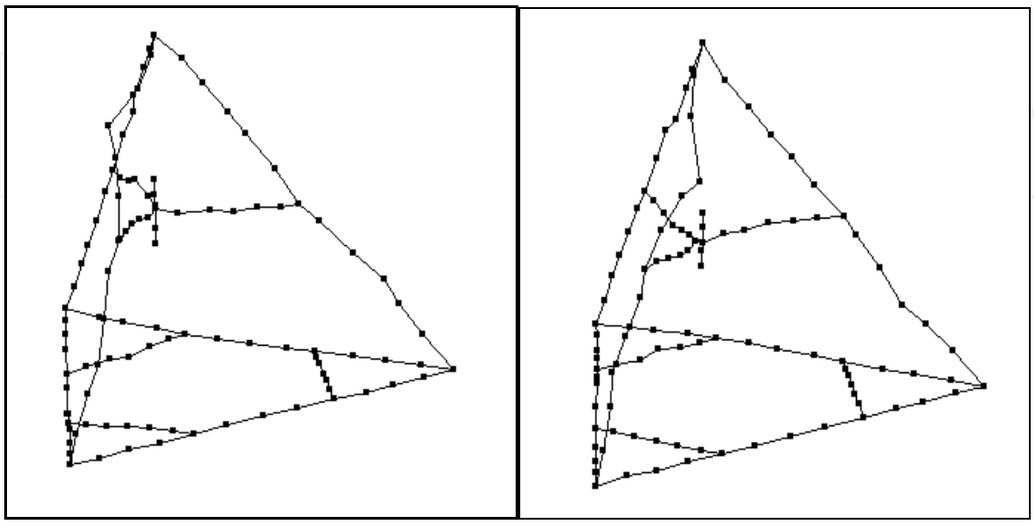

Fig. 19. Me-Scope measured mode shape data (displacement) at a frequency of 3400 Hz.

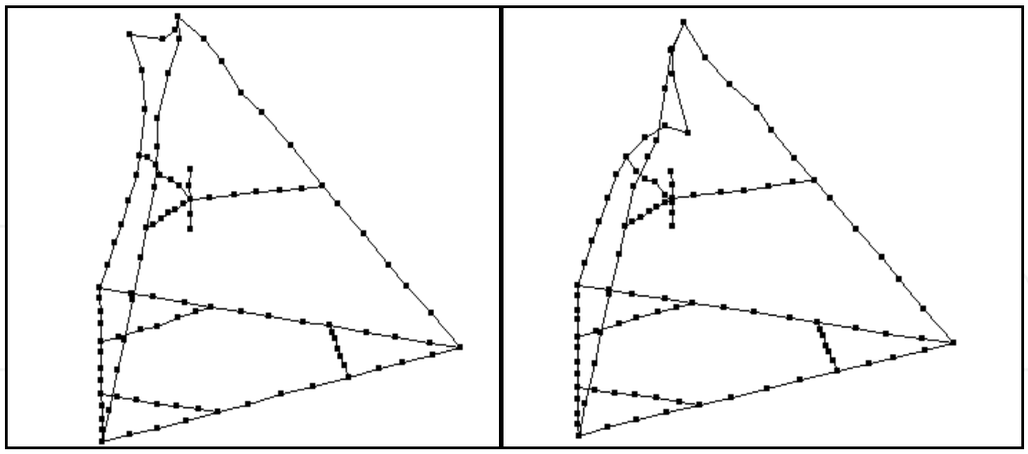

Fig. 20. Me-Scope measured mode shape data (displacement) at a frequency of 4460 Hz.

5. Conclusions

It is concluded that the finite element model prediction compares well with measured data at low frequencies. Owing to this fact, the finite element model may be used for future design improvements to the structure. It can be seen from the experimental and the measurement results that multiple constraints on the spindle enhance the ability of the structure to resist excitation. One possible reason for the structure's oscillation is probably due to the lack of passive damping. Therefore, it is recommended that improvements be made to improve passive damping of oscillations.

6. Acknowledgements

The author thanks Inderscience for use of material that was published as: Dynamic response of a tetrahedral nanomachining machine tool structure by Mark J. Jackson, Luke J. Hyde, Grant M. Robinson, Waqar Ahmed DOI: 10.1504/IJNM.2006.011378, International Journal of Nanomanufacturing, 2006, Volume, Number 1, p.p. 26-46. Full copyright is retained by Inderscience.

7. References

Cook, R. D., *Finite Element Modeling For Stress Analysis*, John Wiley & Sons Inc., New York, 1995.

Inman, D. J., *Engineering Vibration,* Prentice Hall, Upper Saddle River, New Jersey, 2001

Komanduri, R., Chandrasekaran, N., and Raff, L. M., 2001, *Molecular dynamics simulation of the nanometric cutting of silicon,* Philosophical Magazine, B81, 1989-2019.

Luo, X., Cheng, K., Guo, X., and Holt. R., 2003, *An investigation into the mechanics of nanometric cutting and the development of its test bed,* Int. J. Prod. Res., 41, 1449-1465.

Stephenson, D.J., et al: "*Ultra Precision Grinding Using the Tetraform Concept*", Abrasives Magazine, February/March 2002, p.p.12-16.

Vogler, M. E., De Vor, R. E., and Kapoor, S. G., 2001, *Microstructure – level force prediction model for micro-milling of multi-phase materials*, Proceedings of the International Mechanical Engineering Conference and Exposition, A.S.M.E. Manufacturing Engineering Division, 12, p.p., 3 – 10.

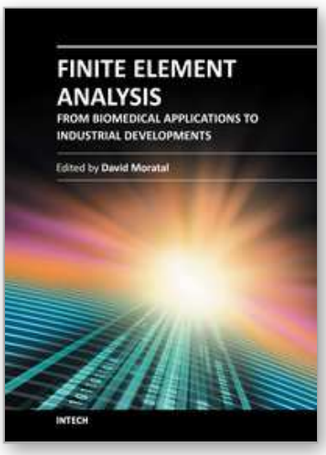

Finite Element Analysis - From Biomedical Applications to Industrial Developments

Edited by Dr. David Moratal

ISBN 978-953-51-0474-2
Hard cover, 496 pages
Publisher InTech
Published online 30, March, 2012
Published in print edition March, 2012

Finite Element Analysis represents a numerical technique for finding approximate solutions to partial differential equations as well as integral equations, permitting the numerical analysis of complex structures based on their material properties. This book presents 20 different chapters in the application of Finite Elements, ranging from Biomedical Engineering to Manufacturing Industry and Industrial Developments. It has been written at a level suitable for use in a graduate course on applications of finite element modelling and analysis (mechanical, civil and biomedical engineering studies, for instance), without excluding its use by researchers or professional engineers interested in the field, seeking to gain a deeper understanding concerning Finite Element Analysis.

How to reference

In order to correctly reference this scholarly work, feel free to copy and paste the following:

M. J. Jackson, L. J. Hyde, G. M. Robinson and W. Ahmed (2012). Finite Element Analysis of Desktop Machine Tools for Micromachining Applications, Finite Element Analysis - From Biomedical Applications to Industrial Developments, Dr. David Moratal (Ed.), ISBN: 978-953-51-0474-2, InTech, Available from: http://www.intechopen.com/books/finite-element-analysis-from-biomedical-applications-to-industrial-developments/finite-element-analysis-of-desktop-machine-tools-for-micromachining-applications

INTECH
open science | open minds

InTech Europe
University Campus STeP Ri
Slavka Krautzeka 83/A
51000 Rijeka, Croatia
Phone: +385 (51) 770 447
Fax: +385 (51) 686 166
www.intechopen.com

InTech China
Unit 405, Office Block, Hotel Equatorial Shanghai
No.65, Yan An Road (West), Shanghai, 200040, China
中国上海市延安西路65号上海国际贵都大饭店办公楼405单元
Phone: +86-21-62489820
Fax: +86-21-62489821

IntechOpen